

Expansion Dynamics of Laser-Generated Si Atomic Beam

Heebyung Chae and Seung Min Park*

Department of Chemistry, Kyung Hee University, Seoul 130-701, Korea

Received December 5, 1996

The generation of atomic and ionic species by laser ablation of solid targets has been studied since the advent of lasers.¹ As solid targets are irradiated by high intensity pulsed lasers, a plume consisting of atoms, ions, molecules, clusters as well as electrons is generated. Since the atomic and molecular species in the plume have high kinetic energies with small angular spread and narrow velocity distribution,² they have good reason to be called as beams. The average kinetic energies of atoms and ions are in the range of tens of electron volt. Such high energy atomic beams with narrow energy distribution will be certainly beneficial to the deposition of thin films. In this regards, there has been a growing interest in the laser ablation of solid targets aiming at the deposition of high quality thin films.³

In particular, laser ablation is now considered as one of the most useful techniques in the stoichiometric deposition of multi-element materials like YBCO superconductors due to its congruent melting characteristics. More recently, pulsed laser ablation has also been proved to be a powerful tool in the deposition of refractory materials since high temperatures well above melting points can easily be obtained.⁴ In case of oxide superconductors and nitrides, the depositions of thin films by laser ablation have been frequently performed in oxygen and nitrogen atmosphere, respectively. Such reactive atmospheres are often required to control the stoichiometry of oxygen or nitrogen of the film deposited. Therefore, it would be highly important to understand the mechanisms of associative chemical reactions giving molecular oxides or nitrides as well as gas phase condensations forming clusters in the reactive laser ablation.

Also, information on the dynamics of laser-induced plume and the transport of the ablated species to the substrate will be of critical importance to understand the details of pulsed laser deposition of thin films. In spite of the very extensive experimental works carried out so far, many phenomena of laser interaction with solid surfaces as well as gas dynamics of the plume are far from satisfactory explanation and still need intensive investigations.⁵ Fundamental details of how the plasma plume is scattered, slowed, and attenuated by background gas collisions are still being revealed. Laser ablation is a very complicated process and there is no reliable model to describe the optical and thermal attributes of the laser ablation as yet.

Recently, we have successfully applied time-resolved optical emission spectroscopy to investigate the laser ablation dynamics of pyrolytic boron nitride in background gas condition.⁶ In this work, we have studied the expansion dynamics of laser-ablated silicon atoms and ions in both high vacuum and background gas conditions employing similar technique. This work has been motivated as preliminary stu-

dies of reactions between laser-ablated silicon atoms and oxygen molecules. Here, we will discuss the validity of molecular beam analogy of laser-generated atomic species and the differences between expansion dynamics in vacuum and background gas conditions.

Experiment

The experimental setup is similar to the one described elsewhere except the laser ablation chamber and signal processing electronics. A high vacuum system with a turbo molecular pump has been built to perform laser ablation experiment in high vacuum condition. The base pressure of the chamber was 8×10^{-8} Torr. The laser ablation was done by the fourth harmonic of Nd : YAG laser (266 nm, Quanta-Ray GCR 150) with pulse duration of 5 ns operating at 10 Hz. Silicon targets with size of 10 mm × 10 mm were used as purchased without further treatment. In the optical time-of-flight (OTOF) experiment, optical emission from laser-generated plume was imaged onto the optical fiber by a lens of 15 cm focal length ($f=3.7$) and sent to a monochromator (SPEX 500M) coupled to a photomultiplier.

The optical fiber was mounted on a 3-dimensional translational stage together with a lens in order to scan the plume region. The photomultiplier signal was averaged and stored in an oscilloscope (300 MHz, LeCroy 9361). Emission spectra were obtained with monochromator, where a boxcar averager (SR250) was used for signal processing. The OTOF measurement was done in high vacuum (2×10^{-5} Torr during laser ablation) as well as in background gas conditions.

The Nd : YAG laser beam was focused onto the target by a lens. The size of the focused laser beam was measured by a single shot on a burn paper. The target was rotated by a standard rotary motion feedthrough. To avoid the aging effect of the target by repetitive irradiation of high intensity laser, targets were frequently replaced to ensure signal reproducibility.

Results and Discussion

Optical emission studies on the laser-generated plume of silicon target have been done both in Ar atmosphere and high vacuum conditions. In high vacuum, the expansion of laser-generated plume is similar to the isentropic expansion of molecular beam.² And the velocity distribution of each atomic species could be described by the theory of molecular beams as shifted Maxwell-Boltzmann distribution:

$$f(v) \propto v^3 \exp[-m(v-v_s)^2/2 kT_s] \quad (1)$$

where v_s is the stream, or center-of-mass velocity and T_s is the effective temperature of the plume.⁷ Conversion of the

*e-mail: smpark@nms.kyunghee.ac.kr

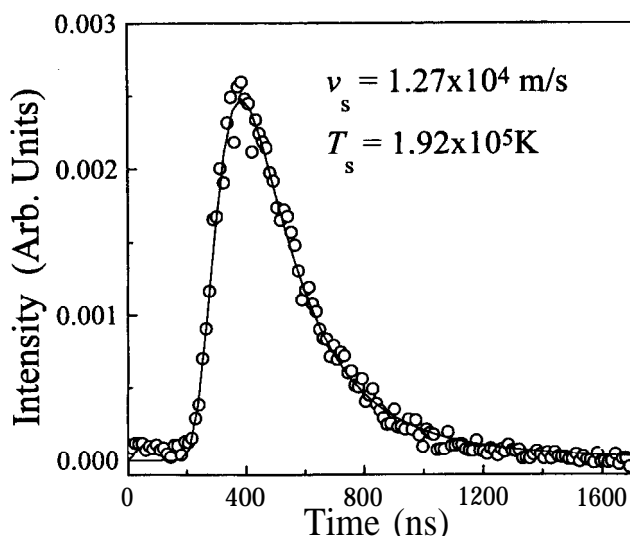


Figure 1. The optical time-of-flight spectrum of Si I at 390.5 nm obtained at laser fluence of 18 J/cm². The solid line is the shifted Maxwell-Boltzmann fit. The pressure was 2 × 10⁻⁶ Torr and the distance between the target and probe was 8 mm.

velocity distribution into a time distribution can be done by using $v=z/t$ where z is the distance from the target to the detector along the plume axis.⁷ Such transformation results in the following function, $N(t)$:⁸

$$N(t) \propto t^{-3} \exp[-m(z/t - v_s)^2/2kT_s] \quad (2)$$

Figure 1 shows the optical TOF spectrum of Si I at 390.5 nm in high vacuum. Solid line is the theoretical curve by Eq. (2), which is in good agreement with the experimental data.

Time-resolved emission intensities at atomic lines corresponding to Si I (390.5 nm) and Si II (412.8 nm) at different distances along the plume axis were measured by moving the optical fiber and lens assembly. Most probable velocities of each species were inferred by plotting the distance versus delay time between the laser pulse and the emission intensity maximum. The scattered laser photons off the target detected by monochromator/PMT via optical fiber had certain delay time with the photodiode trigger signal obtained in front of the laser. Therefore, the scattered laser light detected as described was used as time $t=0$ in the measurement of the delay times of the emission maxima. The inverse of the slope of the line is the most probable velocity of the species⁹ as shown in Figure 2. In vacuum, plume expands without any disturbance or drag forces and the velocities of atomic species show no change as the plume expands. At argon pressure of 100 mTorr which is a typical pressure of reactive laser ablation, however, significant decreases of velocities of both Si I and Si II were observed at near 1.5 mm position. This seems to be due to the change from free expansion to a collision dominated regime.¹⁰ It was found that the shockwave, or ideal blast wave model could be applied to the expansion of the plume at the given pressure. In this model, plasma expansion is given by

$$z = a(t - t_0)^{0.4} \quad (3)$$

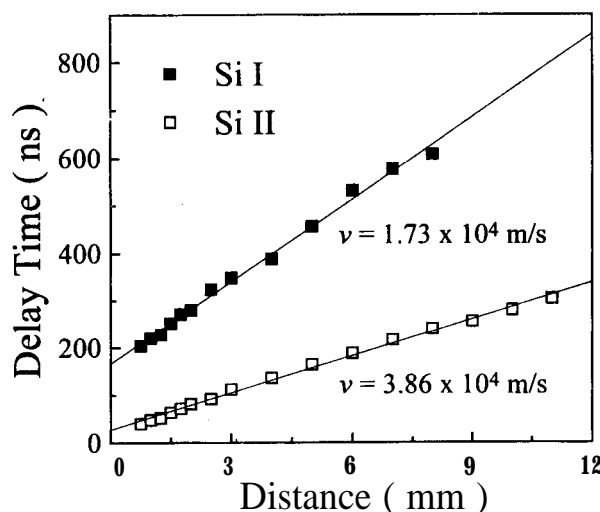


Figure 2. Time delay between the laser pulse and the emission intensity maximum of Si I (390.5 nm) and Si II (412.8 nm) vs. the probe position along the plume axis. The pressure was 2 × 10⁻⁶ Torr and the laser fluence was 12 J/cm². Linear fittings are shown in solid lines.

where z is the distance to the target, t_0 is a zero-time correction factor considering the lifetime of the excited species, and a is a constant at a given pressure.¹⁰

Si II was faster than Si I both in vacuum and argon atmosphere. Due to the long-range Coulomb forces, ions move faster than neutrals.² The Coulomb interaction of the ions by electrons that nearly escape at the plume boundary produces a space-charge field and the ions are accelerated according to their charge by the field.

It is expected that the well-characterized silicon atomic beams with high kinetic energies are generated by laser ablation. The reactions between silicon beams with given kinetic energies and pulsed jet of molecular oxygen in high vacuum will be studied to elucidate the mechanism involved in the formation of silicon oxides in the reactive laser ablation. Such investigations are to be easily expanded to other reactive laser ablations concerning oxide superconductors and refractory nitride materials in the future works.

Conclusion

Time-resolved analysis of the emission intensities observed at different distances from the target gave dynamic information on atomic and ionic species produced by laser ablation. Plume expansion in high vacuum akin to the isentropic molecular beam expansion was observed. At Ar pressure of 100 mTorr, however, the expansion dynamics is better described by the ideal blast wave (shockwave) model. It was found that the shockwave model of laser ablation could be applied even at low background pressures in the early stage of laser ablation.

Acknowledgment. This work has been supported by Basic Research Institute Program, Ministry of Education (Project No. BSRI-96-6401). SMP is also grateful to Korea Science and Engineering Foundation (Grant No. 95-0501-09).

References

1. Singh, R. K.; Narayan, J. *Phys. Rev. B* **1990**, *41*, 8843.
2. Zheng, J. P.; Ying, Q. Y.; Witanachchi, S.; Huang, Z. Q.; Shaw, D. T.; Kwok, H. S. *Appl. Phys. Lett.* **1989**, *54*, 954.
3. Geohegan, D. B. In *Pulsed Laser Deposition of Thin Films*; Chrisey, D. B.; Hubler, G. K. Ed.; Wiley-Interscience: New York, U. S. A., 1995.
4. Polo, M. C.; Cifre, J.; Sanchez, G.; Aguiar, R.; Varela, M.; Esteve, J. *Appl. Phys. Lett.* **1995**, *67*, 485.
5. Amoruso, S.; Berardi, V.; Bruzzese, R.; Capobianco,

- R.; Velotta, R.; Armenante, M. *Appl. Phys. A* **1996**, *62*, 533.
6. Park, S. M.; Shin, K. B.; Kim, Y. M. *Bull. Kor. Chem. Soc.* **1996**, *17*, 416.
7. Stritzker, B.; Pospieszczyk, A.; Tagle, J. A. *Phys. Rev. Lett.* **1981**, *47*, 356.
8. Wolf, P. J. *Appl. Phys. A* **1996**, *62*, 553.
9. Vega, F.; Afonso, C. N.; Solis, J. J. *Appl. Phys.* **1993**, *73*, 2472.
10. Gonzalo, J.; Vega, F.; Afonso, C. N. *Thin Solid Films* **1994**, *241*, 96.

Structural Phase Transformation of Layered Hydroxy Double Salts, $\text{Ni}_{1-x}\text{Zn}_{2x}(\text{OH})_2(\text{CH}_3\text{COO})_{2x} \cdot n\text{H}_2\text{O}$, Depending on Hydration Degree

Jin-Ho Choy*, Young-Mi Kwon, Seung-Wan Song, and Soon Ho Chang †

Department of Chemistry, Center for Molecular Catalysis, Seoul National University, Seoul 151-742, Korea

† Electronics and Telecommunications Research Institute, Taejon 305-600, Korea

Received January 9, 1997

There have been considerable interests in anion-exchangeable layered compounds such as layered hydroxy double salts (HDSs) and layered double hydroxides (LDHs) due to their potential applications to catalysts and ion exchangers.^{1,2} The HDSs have a typical chemical composition of $[(\text{M}^{2+}\text{N}^{2+})_s(\text{OH})_s(\text{A}^{m-})_{2m}] \cdot n\text{H}_2\text{O}$ ($\text{M}=\text{Ni, Co, Zn}$ in octahedral sites, $\text{N}=\text{Cu, Zn}$ in tetrahedral sites) where A is the exchangeable anion such as Cl^- , NO_3^- , etc.^{3,4} In this structure of HDSs, one quarter of octahedral sites in hydroxides layer planes are vacant at a maximum and divalent metal cations tetrahedrally coordinated are stabilized just below and above the empty octahedral sites, which leads to the creation of excess positive layer charge, contrary to LDHs where the surplus layer charge is formed by a partial substitution of trivalent cations for bivalent ones in octahedral sites. Overall charge neutrality is kept on by the presence of exchangeable anions which compensate positive layer charges in the interlayer space. So the structural stability is mainly based upon the electrostatic interaction between layers and anions as well as the hydrogen bonding network among interlayer anions, water molecules, and intralayer hydroxyl groups. In the present study, efforts have been made to investigate the intra- and inter-layer structures of the $\text{Ni}_{1-x}\text{Zn}_{2x}(\text{OH})_2(\text{CH}_3\text{COO})_{2x} \cdot n\text{H}_2\text{O}$ system,⁵ and to discuss the influence of electrostatic interaction between host and guest on the structure. And at the same time, a new route to acetate intercalated HDSs has been proposed, since it is expected to be a good precursor for topotactic anion exchange reaction.

Experimental

Two samples of $\text{Ni}_{1-x}\text{Zn}_{2x}(\text{OH})_2(\text{CH}_3\text{COO})_{2x} \cdot n\text{H}_2\text{O}$ could

*To whom all correspondence should be addressed.

be obtained from nickel-zinc mixed acetate solution by hydrothermal and coprecipitation routes. The concentration of nickel acetate and zinc one in the mixed solution was 0.06 M and 0.04 M, respectively, corresponding to $x=0.25$ in $\text{Ni}_{1-x}\text{Zn}_{2x}(\text{OH})_2(\text{CH}_3\text{COO})_{2x} \cdot n\text{H}_2\text{O}$. The mixed solution was hydrothermally treated at 150 °C for 48 hours under the pressure of 50 atm (hereafter, HT). The resulting green precipitate was separated by centrifuging, washing with decarbonated water, and drying at room temperature. In the coprecipitation (hereafter, CP), this mixed solution and the NH_4OH solution (10 wt.%) were dropwisely added to a flask containing 100 mL of decarbonated water at room temperature. The addition rate of the NH_4OH solution was adjusted to keep pH of the reaction mixture at 9.5. The pH value is included in the optimum synthetic condition of pH=9-12 determined from logarithmic volubility isotherms as shown in Figure 1.^{6,7} The volubility diagram is calculated from the thermodynamic equilibrium constants of nickel and zinc species in aqueous acetate solution listed in Table 1.⁸ In the pH condition with same solubilities of $\text{Ni}(\text{OH})_2$ and $\text{Zn}(\text{OH})_2$, it is expected that the chemical composition of coprecipitate becomes homogeneous and controllable. Therefore, the optimum coprecipitation condition must be determined in the pH domain where both solubilities are the same approximately. In the whole experiments, nitrogen gas was constantly purged into reaction solution to prevent from carbonate contamination. The coprecipitate was aged at 60 °C for 15 hours and separated by centrifuging and washing with decarbonated water, and then dried at room temperature. The final products will be denoted henceforth as HT(t) and CP(t) with air-drying times, t minutes, under relative humidity of 60% at 25 °C. Their powder X-ray diffraction patterns were obtained by Phillips PW 3710 dif-